Title

Experimental analysis of a coiled stirred tank containing a low cost PCM emulsion as a thermal energy storage system

Authors

M. Delgado[1,]*, A. Lázaro[1], J. Mazo[1], C. Peñalosa[1], J.M. Marín[1], B. Zalba[1]

Aragón Institute for Engineering Research (I3A), Thermal Engineering and Energy Systems Group, University of Zaragoza

Agustín Betancourt Building, C/María de Luna 3, 50018 Zaragoza, Spain

Phone: (+34) 876 555 584

*Corresponding author: monica@unizar.es

Keywords

PCM slurry; PCM emulsion; Stirred tank; Thermal Energy Storage density

Highlights

- A coiled stirred tank with a low cost PCM emulsion has been experimentally analysed
- It improves the storage efficiency, achieving the maximum storage capacity
- The overall heat transfer coefficient is 4 times higher due to the agitation
- The overall heat transfer coefficient reaches similar values to those of conventional water tanks

Abstract

This article presents the results of heat transfer coefficient and volumetric energy density measurements in an agitated tank containing a low-cost phase change material emulsion, heated by water flowing in a coil. For the stirring a three-stage impeller is placed in the central axis of a 46 l commercial tank. By measuring the temperature dependency on time and solving the transient enthalpy balance, the heat transfer coefficient between the helical coil and the agitated phase change material emulsion is determined, based on the impeller Reynolds number. The thermal energy

storage efficiency has also been analysed. This phase change material emulsion shows a phase change temperature range between 30 and 50ºC. Its solid content is about 60% with an average size of 1 µm. The results have shown that the overall heat transfer coefficient is around 3.5-5.5 times higher when a stirring rate of 290-600 rpm is used. Furthermore, even at the lowest stirring rate, the thermal energy storage efficiency improves from 76-77% to 100%, without detriment to the energy consumption of the stirrer.

Nomenclature

A	Heat transfer area (m^2)
C_{min}	Minimum heat capacity (kJ/K)
c	Specific heat capacity (kJ/(kg·K))
D	Vessel diameter (m)
D_H	Helical coil diameter (m)
d	Diameter (m)
E	Energy (kJ)
F	Correction factor for the average temperature difference in heat exchangers (-)
H	Liquid height (m)
h	Convective coefficient (W/(m^2·K)); Enthalpy (kJ/kg)
L	Characteristic length (m)
L_c	Length of the coil (m)
l_i	Position along the coil (m)
$\dot{m}$	Mass flow rate (kg/s)
m	Mass (kg)
N	Stirring rate (s^{-1})
$\dot{Q}$	Heat (W)
T	Temperature (ºC)
t	time (s)
t_d	Dwell time (s)

U Overall heat transfer coefficient (W/(m^2·K))

v Heat transfer fluid speed (m/s)

V Volume (m^3)

ΔT Temperature difference (ºC)

x Position (m)

Greek symbols

$\dot{\gamma}$ Shear rate (s^{-1})

ε Effectiveness (-)

ε_{TES} Thermal Energy Storage efficiency (-)

λ Thermal conductivity (W/(m·K))

μ Dynamic viscosity (Pa·s)

ρ Density (kg/m^3)

τ Time integration variable (s)

φ_i Basis function of the piecewise interpolation space

Abbreviation

HTF Heat Transfer Fluid

NRMSD Normalized Root-mean-squared deviation

PCM Phase Change Material

TES Thermal Energy Storage

Dimensionless numbers

De Dean number (-)

N_p Power number (-)

Nu	Nusselt number (-)
Pr	Prandlt number (-)
Ra	Rayleigh number (-)
Re	Reynolds number (-)

Subscripts

0	Relative to an initial situation
amb	Ambient, room
ext	External
imp	Impeller
in	Inlet
i,j	Natural numbers
int	Internal
m	Mean, average
ml	Mean logarithmic
out	Outlet
w	Wall

1. Introduction

PCM slurries have been widely studied because of their potential contribution to sustainable energy models. The first studies were mainly focused on their use as heat transfer fluids, while the most recent studies have experimentally studied tanks containing PCM slurries as thermal storage material, with water as a HTF flowing through a spiral type internal heat exchanger [1-3], through an external plate heat exchanger [4-5], or through a tube-bundle heat exchanger [6].

A previous work by the present authors addressed a tank containing a low-cost phase change material emulsion as thermal storage material, and a helical coil as heat exchanger, through which water flowed as HTF [7]. The aim of this work was to analyse the volumetric energy density and the heat transfer during the charging and discharging processes, two important criteria when designing TES systems. Furthermore, these parameters were compared to those of sensible TES systems, and to more conventional latent TES systems, where the PCM is macroencapsulated or directly confined. It was observed that although the TES systems with PCM slurries were not competitive against the sensible systems with water in terms of their overall heat transfer coefficient, they did show significant improvements over traditional latent systems. However, these PCM slurry systems had a lower A/V ratio, which was detrimental to the thermal power. These systems had a higher energy density than the water systems, but slightly lower than some conventional latent systems. The improvement in terms of the energy density of the system was not as great as expected because of the non-specific design of the tank, resulting in dead volumes which did not undergo complete melting during a time period practical for an engineering application.

In light of these previous results, the inclusion of a stirrer in the tank is contemplated in the present research as a potential measure to improve its performance by reducing the temperature gradient. The stirrer would significantly increase the motion of the emulsion inside the tank, boosting the convection and avoiding dead volumes. This approach is addressed in reference [8], where the thermal performance of a coil-in-tank containing a microencapsulated PCM slurry was experimentally investigated and compared to a tank containing water. It was observed that the volumetric energy density of the latent system was twice that of the water thanks to the agitation induced by the stirrer. It was also observed that the external forced convective heat transfer coefficient could be several times higher than for water, especially in the phase change temperature range from an angular velocity of 280 rpm.

The present work has also adopted this solution in order to promote the convection and to improve the thermal energy storage efficiency. The same TES system tested previously [7] by the authors has been experimentally analysed, but with the inclusion of a stirrer controlled by a variable frequency drive.

2. Materials and properties

As in the previous work [7], a PCM emulsion has been analysed in which the emulsified PCM is a low-cost paraffin, specifically a by-product of the petroleum refining process. This PCM emulsion is in turn a co-product, since to date it has been used for other purposes unrelated to the purpose presented here. According to the technical specifications supplied by the manufacturer, the solid content of this PCM emulsion is about 59-61%, with an average particle size of 1 µm. In spite of being the same product as that employed in the previous work, it has been characterized again to check possible differences in the thermophysical and rheological properties given that different batches of the product are used. No significant changes were observed.

3. Heat transfer study of a stirred tank for use as thermal storage material

3.1 Description of the experimental installation

A new storage tank was supplied by the Spanish manufacturer Lapesa, identical to the previously tested tank, the only difference being the thickness of the insulation, requiring a repetition of the characterization of the heat losses to the ambient air. The tank volume is 46 litres, its internal diameter 29.5 cm and its length 83.5 cm. It has an internal coil working as a heat exchanger, whose internal diameter is 23 mm. The wall thickness is 1 mm and the heat exchange surface 0.71 m^2. The tank was isolated with polyurethane with a thickness of 3 cm.

A stirrer was installed in the upper part at the central axis of the storage tank. The stirrer, supplied by the manufacturer Vak Kimsa, consists of three different elements: a 0.37 kW motor; a mixing shaft with a length of 740 mm and a diameter of 25 mm including a three stage trilight impeller [9] having a diameter of 125 mm; and a frequency drive, which allows the angular velocity to be varied from 290 rpm to 940 rpm.

The HTF is water which enters the coil through the lower part and leaves through its upper part. Two 4 wire-Pt100 sensors were used to measure the water temperature at the inlet and outlet of the coil. These resistance temperature sensors are mineral insulated, 1/3 DIN, with a stainless steel sheath with a diameter of 3 mm and a length of 180 mm. The sensors were placed in parallel to the tube through an adjustable compression fitting. Both temperature sensors were calibrated at three temperature levels: 25, 50 and 75ºC. The maximum deviation observed in these sensors according to the calibration report is 0.04ºC.

In the previous work, the temperature of the PCM emulsion was measured along the central axis of the tank, having placed for that purpose 7 Pt100 sensors at equidistant intervals. For a rigorous comparison, these sensors should ideally have been spatially arranged in the same manner. However, due to the presence of the mixing shaft and arrangement of the impellers, new flexible Pt100 sensors were purchased to avoid these spatial obstacles. Their technical specifications were the same as those used in the prior installation, and the same as those used for the temperature measurement of the HTF, with the exception that they can be bent along their length. These temperature sensors were also calibrated at three temperature levels: 25, 50 and 75ºC, observing in this case a maximum deviation of 0.07ºC. The sensors were placed in the tank using seven single sensor feed-through sealing assemblies, passing through the flange and the stirrer head. The detail of the arrangement can be observed in figure 1. The sensors were placed in such a way that the first sensor was at 105 mm down from the upper part and the next five, 105 mm spaced one from each other. The seventh sensor is placed at 150 mm from the previous one. All the sensors were arranged radially in a range of 21 mm from the central axis. For the seven measurement points, the immersion depth was higher than the minimum immersion depth required by the calibration tests.

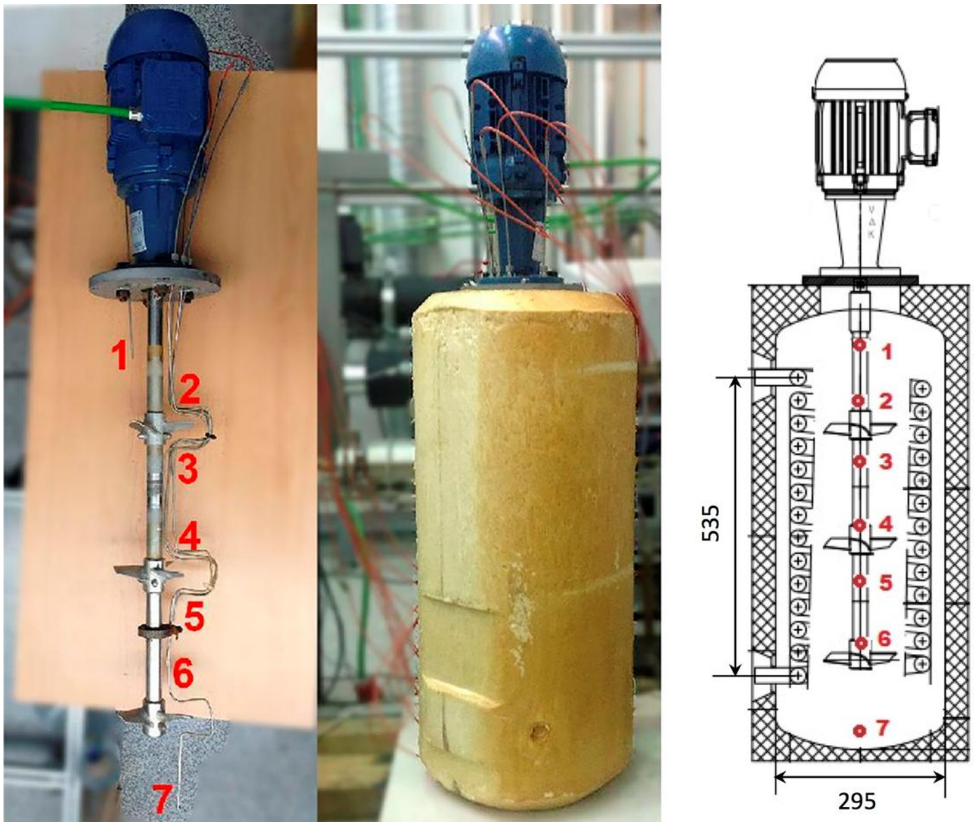

Figure 1. Arrangement of the Pt100 sensors inside the tank

The mass flow rate measurement of the HTF was carried out with a Coriolis mass flow meter, which has an accuracy of 0.1% for liquids. The establishment of the initial conditions of the tank, as well as the flow temperature of the HTF, was controlled by a thermostatic bath, a Hüber model Unichiller UC40T-H. Its temperature stability is 0.1 K. Further technical details of the installation to which the tank was connected can be found in a previous article by Delgado et al. [10].

3.2 Tests using water as thermal storage material

Heating tests were performed using water both as HTF and as TES material. The temperature levels were selected according to the phase change temperatures of the PCM emulsion to be analysed. The initial temperature of the stored water was 30ºC and the flow temperature of the water as HTF was 60ºC. The mass flow was selected according to the maximum pumping of the thermostatic bath, approximately 400 kg/h.

Figure 2 shows the temperature evolution of the water stored in the tank. The temperature increases, and no significant temperature differences between the measurements of the sensors from position 1 to position 6 were observed. However, the temperature in the lower part of the tank, recorded by the sensor in position 7, remained constant during the test. This is due to the fact that the volume of water corresponding to the measurement of this probe is located below the coil. The heat transfer towards this section is predominantly by conduction and not by convection, giving rise to this dead volume. This phenomenon was also observed in the previous work [7].

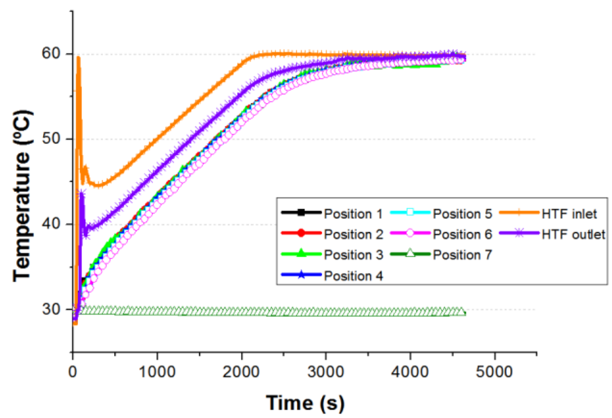

Figure 2. Temperature evolution of the HTF at the inlet and outlet of the coil and temperature evolution of the water inside the tank along the central axis. Flow temperature=60ºC; Mass flow=400 kg/h. No stirring.

The same test was carried out but this time stirring the water contained in the tank at four different angular velocity levels, from the minimum possible angular velocity, 290 rpm, up to 600 rpm. Figure 3 shows the temperature evolution with stirring at 290 rpm. As can be observed, due to the motion caused by the stirrer, the heating rate of the water in region 7 is equal to the rest of the regions, avoiding the dead volume previously observed in figure 2. A shorter time is needed to reach the set temperature of 60ºC, implying an improvement in the heat transfer rate. It is also observed that the HTF outlet temperature is almost the same as the water tank temperature, which shows the improvement in the heat exchanger effectiveness.

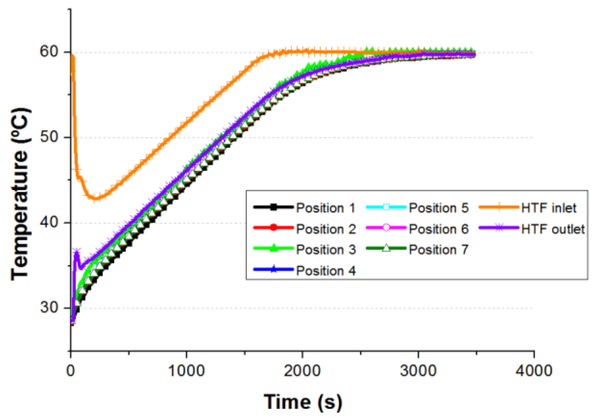

Figure 3. Temperature evolution of the HTF at the inlet and outlet of the coil and temperature evolution of the water inside the tank along the central axis. Flow temperature=60ºC; Mass flow=400 kg/h. Stirring at 290 rpm.

3.2.1 Obtaining the overall heat transfer coefficient

Due to the characteristics of the transient response of the experimental installation during the tests, the transient phenomena in the heat transfer fluid account for an appreciable contribution (around 8%). Consequently, a data processing method based on the analytical solution of a transient heat transfer model of the tank has been proposed. This mentioned model is founded on the following assumptions:

- The axial conduction heat transfer in the water and in the tubes is neglected
- The overall heat transfer coefficient, U, is uniform and the thermo-physical properties and the mass flow of the heat transfer fluid are constant
- The thermal energy variation of the tube wall is neglected

According to these simplifications, the transient heat transfer process can be modelled by the following linear first order partial differential equation (equations 1, 2 and 3).

$$\frac{1}{v} \cdot \frac{dT(x,t)}{dt} + \frac{dT(x,t)}{dx} = \frac{NTU}{L_c} \cdot (T_{TES}(t) - T(x,t)) \quad \text{(eq. 1)}$$

$$T(x = 0, t) = T_{in}(t) \quad \text{(eq. 2)}$$

$$T(x, t = 0) = T_o(x) \quad \text{(eq. 3)}$$

The solution to the partial differential equation is presented below [11] (equation 4):

$$T(x,t)=\begin{cases} T_0(x-v\cdot t)\cdot e^{-\frac{NTU}{L_c}\cdot v\cdot t}+\frac{NTU\cdot v}{L}\cdot e^{-\frac{NTU}{L_c}\cdot v\cdot t}\cdot\int_{\tau=0}^{\tau=t}T_{TES}(v\cdot\tau,\tau)\cdot e^{\frac{NTU}{L_c}\cdot v\cdot\tau}\cdot d\tau & v\cdot t-x\le 0\\ T_{in}\left(t-\frac{x}{v}\right)\cdot e^{-\frac{NTU}{L_c}\cdot x}+\frac{NTU\cdot v}{L}\cdot e^{-\frac{NTU}{L_c}\cdot x}\cdot\int_{\tau=0}^{\tau=\frac{x}{v}}T_{TES}\left(v\cdot\tau,t-\frac{x}{v}+\tau\right)\cdot e^{\frac{NTU}{L_c}\cdot v\cdot\tau}\cdot d\tau & v\cdot t-x>0\end{cases}$$

(eq. 4)

This analytical solution is used to calculate the overall heat transfer coefficient from the registered evolution of the temperature at the inlet and outlet of the tube, $\{T_{in,i}\}$, $\{T_{out,i}\}$, and the temperature of the TES fluid, $\{T_{TES,j,i}\}$, at different points $\{j\}$ (figure 1). Some additional simplifications concerning the initial conditions can be introduced to the general expression of the analytical solution (equation 4). According to this, if during the first dwell time ($t_d=\frac{L_c}{v}$) [12] the following conditions are verified (equation 5), equation 6 represents the solution to the partial difference equation (defined by equations 1, 2 and 3).

$$T(x,t=0)=T_{TES}(x,t)=T_0 \qquad 0\le t\le t_d \quad \text{(eq. 5)}$$

$$T(x,t)=\begin{cases} T_0 & v\cdot t-x\le 0\\ T_{ent}\left(t-\frac{x}{v}\right)\cdot e^{-\frac{NTU}{L_c}\cdot x}+\frac{NTU\cdot v}{L_c}\cdot e^{-\frac{NTU}{L_c}\cdot x}\cdot\int_{\tau=0}^{\tau=\frac{x}{v}}T_{TES}\left(v\cdot\tau,t-\frac{x}{v}+\tau\right)\cdot e^{\frac{NTU\cdot v}{L_c}\cdot\tau}\cdot d\tau & v\cdot t-x>0\end{cases}$$

(eq. 6)

Equation 7 represents the evolution of the temperature at the outlet of the coil. Once the first dwell period has taken place, it relates the transient evolution of the temperature at this point, on the one hand, to the evolution of, respectively, the dwell-time delayed inlet temperature, and the distribution of TES fluid temperature and, on the other hand, to the heat exchange conditions -represented by the number of transfer units, (NTU).

$$T_{out}(t)=\begin{cases} T_0 & 0\le t<\frac{L}{v}\\ T_{in}(t-t_d)\cdot e^{-NTU}+\frac{NTU}{L_c}\cdot v\cdot e^{-NTU}\cdot\int_{\tau=0}^{\tau=\frac{L}{v}}T_{TES}(v\cdot\tau,t-t_d+\tau)\cdot e^{\frac{NTU}{L_c}\cdot v\cdot\tau}\cdot d\tau & \frac{L}{v}\le t\end{cases}$$

(eq. 7)

In order to deal with experimental data, a piecewise linear function (equation 8) is built from the registered temperatures of the TES fluid in the tank at different points (figure 1) with the purpose of describing the corresponding temperature distribution along the coil.

$$T_{TES}(v\cdot\tau,t-t_d+\tau)=\sum_{j=1}^{6}T_{TES,j}\left(t-\frac{L_c-l_j}{v}\right)\cdot\varphi_j(\tau) \quad \text{(eq. 8)}$$

In equation 8, l_j (m) represents the corresponding position along the coil of the measured temperature of the tank, $T_{TES,j}$. In order continue with the following steps, equation 8 can be rearranged into equation 9 (provided that $l_1 = 0$). The temperatures at each instant $t_i - t_d \cdot \frac{L_c - l_j}{L_c}$ are calculated by the linear interpolation of experimental data.

$$T_{TES,t_i}(\tau) = T_{TES,1,t_i-t_d} + \sum_{j=2}^{6}\left(T_{TES,j,t_i-t_d\cdot\frac{L_c-l_j}{L_c}} - T_{TES,1,t_i-\Delta t}\right)\cdot\varphi_j(\tau) = T_{TES,1,t_i-t_d} +$$

$$+\sum_{j=2}^{6}\Delta T_{TES,j,t_i-t_d\cdot\frac{L_c-l_j}{L_c}}\cdot\varphi_j(\tau) \qquad \text{(eq. 9)}$$

From the analysis of equation 7, it can be concluded that no information about the NTU during the first dwell time can be obtained. However, after this first period the following implicit relation (equation 10) can be stablished between this dimensionless number and the measured evolution of the temperatures.

$$NTU = ln\left(\frac{T_{in,t_i-\Delta t} - T_{TES,1,t_i-t_d}}{T_{out,t_i} - T_{TES,1,t_i-t_d} - \overline{\Delta T}_{TES,t_i}}\right) \qquad t_i > t_d \quad \text{(eq.10)}$$

Where the temperature difference $\overline{\Delta T}_{TES,t_i}$ of equation 10 is calculated from equation 11.

$$\overline{\Delta T}_{TES,t_i} = \frac{NTU}{L_c}\cdot e^{-NTU}\cdot\sum_{j=2}^{6}\Delta T_{TES,j,t_i-t_d\cdot\frac{L_c-l_j}{L_c}}\cdot\int_0^{L_c} e^{\frac{NTU}{L}\cdot x}\cdot\varphi_j(x)\cdot dx \quad \text{(eq.11)}$$

Equation 10 is solved by means of a fixed point iteration [13] at each time step t_i with a relative tolerance of 10^{-12}. Figure 4 shows the overall heat transfer coefficient obtained at every instant during the transient response of the tests of figure 2 and figure 3. The error band associated to the propagation of the uncertainty in the measurements, detailed in section 3.1, is also plotted in the figure. The overall heat transfer coefficient with stirring at 400, 500 and 600 rpm is also displayed in the graph. Due to the increased convection, the overall heat transfer coefficient increases by 2.14-2.92 times.

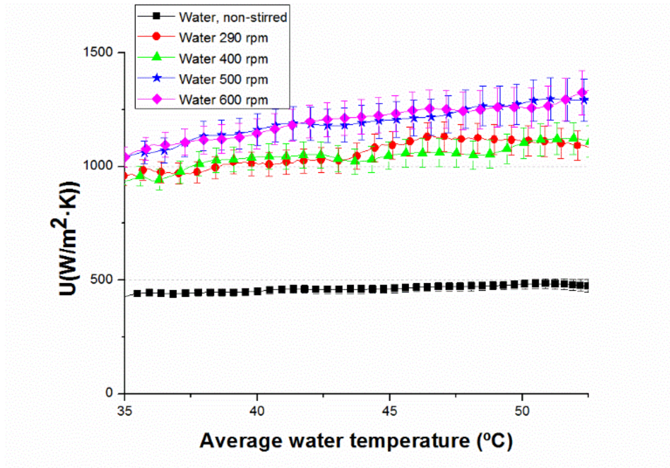

Figure 4. Overall heat transfer coefficients for the water without stirring (natural convection) and stirring at 290, 400, 500 and 600 rpm.

3.2.2 Analysis of the external convective heat transfer coefficient: comparison with correlations provided in the literature

Once the overall heat transfer coefficient U has been determined, the heat transfer coefficient in the stored water, external to the coil (h_{ext}), can be obtained by means of an analysis of the thermal resistances, and by calculating from correlations the internal forced heat transfer coefficient in the helical coil. Equation 12 shows the equation from the thermal resistance analysis:

$$\frac{1}{U} = \frac{1}{h_{ext}} + \frac{d_{ext}}{2\cdot\lambda}\cdot ln\left(\frac{d_{ext}}{d_{int}}\right) + \frac{d_{ext}}{d_{int}}\cdot\frac{1}{h_{int}} \quad \text{(eq. 12)}$$

To calculate the convective heat transfer coefficient in the inner part of the helical coil h_{int}, firstly the critical Reynolds number has been calculated to identify the flow regime of the water flowing inside the coil. The Ito equation [14] (equation 13) has been used, the critical Reynolds number being 9420.

$$Re_{critical} = 20000\left(\frac{d_{int}}{D_H}\right)^{0.32} \quad \text{(eq. 13)}$$

According to the critical Reynolds number, the water flows under laminar flow conditions (under the maximum mass flow that the thermostatic bath provides). Once the flow regime was determined, one of the correlations compiled in Naphon and Wongwises's review [15] was selected, namely, the correlation proposed by Xin and Ebadian [16] (equation 14) that gives the average internal forced convection coefficient in the completely developed region. The properties of water were calculated at its average temperature at the inlet and outlet of the coil.

$$Nu_{int} = (2.153 + 0.318 \cdot De^{0.643}) \cdot Pr^{0.177}$$

$$20<De<2000; \quad 0.7<Pr<175; \quad 0.0267<d_{int}/D_H<0.0884 \quad \text{(eq. 14)}$$

In our previous investigation [7], the natural convective coefficients were obtained for the stored water without motion so as to subsequently calculate the Nu_D-Ra_D values and thus check the results with previous correlations provided by other authors. The same approach has been adopted for the tests executed with water as thermal storage material at different stirring levels, in order to check the new results.

The heat transfer rate between the helical pipe coil and the agitated liquid depends on many parameters, such as the tank-coil-impeller geometry, the agitated liquid properties, and the mixing intensity, which is influenced by the type of agitator and its rotation rate. Dimensionless parameters are generally used to describe this relation between the heat transfer coefficient and these other parameters. The relation is usually written as shown by equation 15:

$$Nu = f(Re, Pr, geometry) \quad \text{(eq. 15)}$$

with the following definitions of the impeller Reynolds [17] and Nusselt numbers (equation 16):

$$Re \equiv \frac{N \cdot d_{imp}{}^{2} \cdot \rho}{\mu}; \quad Nu \equiv \frac{h \cdot L}{\lambda} \quad \text{(eq. 16)}$$

Due to the uniformity of the temperature field when stirring is in progress, the properties have been calculated at the average water temperature. This average temperature was weighted, based on the mass of each section.

When the heat transfer process in the agitated vessel takes place by the use of the coil, either the diameter of the agitated vessel, or the outer diameter of the coil tube or the coil diameter is taken as the characteristic length [18]. In the present study, the diameter of the vessel has been considered as the characteristic length. The Nusselt number has been calculated from the external forced convective coefficient between the agitated liquid and the helical pipe coil obtained during the transient response of the tests. Furthermore, the relation appears in the literature with an additional term, the Sieder-Tate correction factor, representing the change in the thermophysical properties of liquid near the heat transfer wall. In this way, this relation can adopt the form of equation 17. Most researchers have put forward correlations with this form [19].

$$Nu_{ext} = c \cdot \mathrm{Re}^{m} \cdot \mathrm{Pr}^{n} \cdot \left(\frac{\bar{\mu}}{\mu_w} \right)^{s} \quad \text{(eq. 17)}$$

where the Prandlt power n is commonly given as 1/3, and the Sieder-Tate correction term power s is usually 0.14 [20]. Taking these two exponents and the results of testing at different rotation velocities, a set of values of these dimensionless numbers has been obtained. The values have been fitted by least squares to the relation provided by equation 17, giving as a result the correlation shown in equation 18, with a NRMSD=9.2%. Figure 5 shows the experimental results, with their associated uncertainty caused by measuring errors and the accuracy of the correlation for the internal forced convection that has been used, in comparison to the fitting results.

$$Nu_{ext} = 0.74 \cdot Re^{0.59} \cdot Pr^{1/3} \cdot \left(\frac{\bar{\mu}}{\mu_w} \right)^{0.14}$$

$$1 \cdot 10^5 \le Re \le 3 \cdot 10^5; \quad 3.0 \le Pr \le 5.7; \quad H/D=2.45; \quad D/d_{impeller}=2.40 \quad \text{(eq. 18)}$$

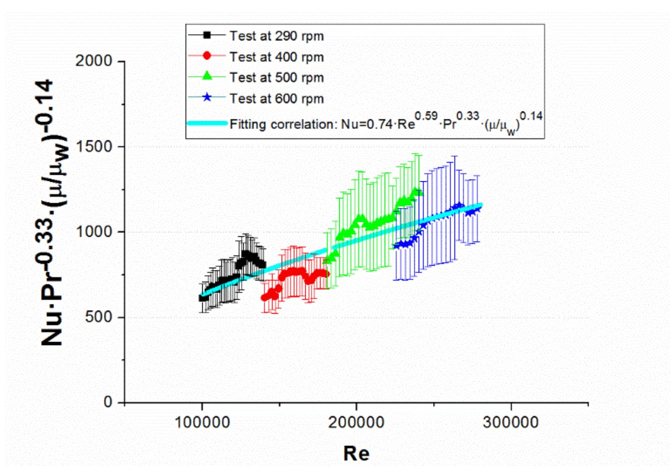

Figure 5. Dimensionless experimental results vs.fitting correlation.

It turns out to be difficult to validate this correlation with correlations provided in the literature, as geometrically similar vessels should be compared. Values of the other characteristic geometric dimensions of the coil, impeller and vessel should be checked in this comparison or be included in the correlation, in addition to further aspects such as the type of impeller, off-center impeller positions, the tank shape or whether there are multiple impellers, among others. In this case, the fitting correlation was simply compared to other correlations found in the literature [21] to check if the values obtained are reasonable within a certain range, bearing in mind that completely different systems are being compared. Figure 6 shows this comparison, having included different types of impeller (paddle, propeller, anchor). In light of this comparison, it can be stated that the results with water are consistent, even though they are slightly lower than those given for the other impellers.

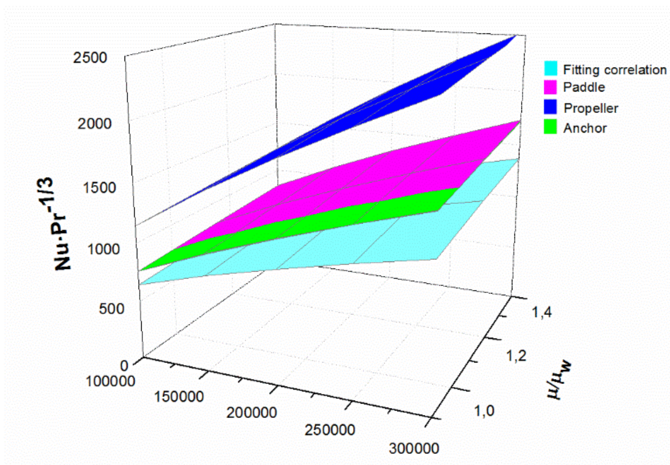

Figure 6. Comparison of the fitting correlation with other correlations taken from the literature.

*The correlation for the paddle impeller is not visible, because it is overlapped by the correlation for the anchor impeller.

3.2.3 Energy stored by the TES system with water

To calculate the energy stored by the tank, the energy balance on the system should be obtained according to equation 19:

$$E_{tank\ stored}(t) = E_{coil}(t) + \int_0^t \left(\dot{Q}_{imp} - \dot{Q}_{amb}\right) \cdot dt \quad \text{(eq. 19)}$$

First of all, equation 20 has been used for the evaluation of the amount of thermal energy which is transferred to the fluid in the tank, $E_{coil}(t)$. Besides, equation 21 represents the numerical method which has been applied to the experimentally registered data.

$$E_{coil}(t) = \int_0^t \dot{m}\cdot c_p \cdot \left(T_{in}(t) - T_{out}(t)\right)\cdot dt + \frac{\dot{m}\cdot c_p}{v}\cdot\int_0^{L_c}\cdot\left(T(x,t) - T_0(x)\right)\cdot dx \quad \text{(eq. 20)}$$

$$E_{coil}(t_N) = \dot{m}\cdot c_p \cdot \left[\sum_1^N \frac{T_{in}(t_i)+T_{in}(t_{i-1})-T_{out}(t_i)-T_{out}(t_{i-1})}{2}\cdot \Delta t_i + (\bar{T}(t_N) - T_0)\cdot t_d\right] \quad \text{(eq. 21)}$$

The average temperature of the heat transfer fluid $\bar{T}(t)$ can be calculated from the integration of equation 1 thus resulting in equation 22.

$$\bar{T}(t_i) = \bar{T}_{TES}(t_i) - \frac{T_{out,t_i} - T_{in,t_i-t_d}}{U\cdot A} - \frac{\int_0^{L_c}\frac{\partial T}{\partial t}\cdot dx}{U\cdot A\cdot v} \quad \text{(eq. 22)}$$

The definite integral of the last term of equation 22 is calculated using the analytical solution (equation 6) of the heat transfer model which is proposed in section 3.2.1. Here an approximation to the time evolution of the temperatures at the inlet of the water flow and in the tank is introduced: it is assumed that the evolution of these temperatures can be linearly approximated in the time interval $[t_i - t_d, t_i]$ (equations 23 and 24).

$$T_{in}(t) = T_{in,t_i-t_d} + \left(T_{in,t_i} - T_{in,t_i-t_d}\right)\cdot\frac{t-t_i}{t_d} \qquad t_i - t_d < t \leq t_i \quad \text{(eq. 23)}$$

$$T_{TES}(x,t) = T_{TES,t_i-t_d}(x) + \left(T_{TES,t_i}(x) - T_{TES,t_i-t_d}(x)\right)\cdot\frac{t-t_i}{t_d} \qquad t_i - t_d < t \leq t_i \quad \text{(eq. 24)}$$

Using these approximate functions, the average temperature of the heat transfer fluid can be calculated by equation 25 from the experimental data, $\{T_{in,i}\}$, $\{T_{out,i}\}$ and $\{T_{TES,j,i}\}$.

$$\bar{T}_{t_i} = \begin{cases} T_0\cdot\left(1-\frac{1}{NTU}\right) + \frac{1}{NTU}\cdot\left[T_{in,i} - \left(T_{in,i} - T_0\right)\cdot\frac{1-e^{-\frac{NTU}{L}\cdot v\cdot t}}{NTU}\right] & t_i \leq t_d \\ \bar{T}_{TES,t_i} - \frac{\bar{T}_{TES,t_i} - \bar{T}_{TES,t_i-t_d}}{NTU} + \frac{1}{NTU}\cdot\left[T_{in,t_i} - T_{out,t_i} - \frac{T_{in,t_i} - T_{in,t_i-t_d} - \left(T_{out,t_i} - T_{out,t_i-t_d}\right)}{NTU}\right] & t_i > t_d \end{cases}$$

(eq. 25)

The average temperature of the tank in equation 25, $\bar{T}_{TES,t_i}$, is calculated from experimental data using equation 26.

$$\bar{T}_{TES,t_i} = \sum_{j=1}^6 T_{TES,j}\left(t - \frac{L_c - l_j}{v}\right)\cdot\bar{\varphi}_j(\tau) = \frac{l_2 - l_1}{2\cdot L_c}\cdot T_{TES,1} + \sum_{j=2}^5 \frac{l_{j+1} - l_{j-1}}{2\cdot L_c}\cdot T_{TES,j} + \frac{l_6 - l_5}{2\cdot L_c}\cdot T_{TES,6}$$

(eq. 26)

Secondly, it is necessary to estimate the heat losses from the tank to the ambient air. In spite of the tank being the same as that of the previous study [7], the insulation thickness of the new tank is lower. Thus, a test was carried out in which the water contained in the tank was heated up to a temperature of 60ºC. Once 60ºC was reached, the water supply through the coil was stopped, and the water temperature evolution and the room temperature were recorded. From the energy balance on the tank (equation 27), an overall heat loss coefficient was obtained:

$$\frac{dE_{water}}{dt}+\frac{dE_{insulation}}{dt}+\frac{dE_{stainlesssteel}}{dt}=\dot{m}\cdot c\cdot(T_{in}-T_{out})-\dot{Q}_{amb} \text{ (eq. 27)}$$

Since the temperature evolution of the different elements of the tank is not known, and the storage capacity of these elements (insulation and stainless steel parts) is very low in comparison to the total heat capacity (lower than 5% when testing water as thermal storage material), only the energy stored by the water is taken into account to calculate this overall heat loss coefficient. From equation 28, the coefficient U_{loss} can be obtained:

$$\dot{Q}_{amb}=U_{loss}\cdot A_{tank}\cdot(T_{water}-T_{amb}) \text{(eq. 28)}$$

The values obtained were adjusted to a correlation type $U=c\cdot\Delta T^{m}$, obtaining equation 29, where ΔT is defined by equation 30. The water temperature is the average temperature of the water contained by the tank provided by the seven temperature sensors, which has been weighted based on the mass of each section. The heat losses to the ambient are at all times lower than 3% of the heat exchanged by the coil, therefore it can be neglected when the stored energy is calculated.

$$U_{loss}=0.478\cdot\Delta T^{0.320} \text{(eq. 29)}$$

$$\Delta T=T_{water}-T_{amb} \text{(eq. 30)}$$

In the same manner, the heat dissipated by the mechanical energy of the impeller should be calculated. The mechanical energy is transferred from the impeller to the fluid, causing fluid motion. The energy then dissipates in the fluid in the form of thermal energy. To take into account this heat flow in the present work, an energy balance has been made on the stirred tank (equation 31) to estimate the power dissipated at the different stirring rates and for both water and the PCM emulsion. This method is also used to estimate the power consumption of the stirrer, although the losses due to friction in the bearings and other mechanical devices should be considered [22].

$$\frac{dE_{water}}{dt} = \dot{Q}_{imp} - \dot{Q}_{amb} \quad \text{(eq. 31)}$$

Following this procedure with water showed that the heat dissipated was 6.5, 12.5 and 21.5 W at 400, 500 and 600 rpm respectively. These values have been satisfactorily checked, since the manufacturer has provided us the Power number-Reynolds number curve for our type of impeller. The Reynolds and the Power numbers were calculated according to equations 32 and 33 [17], respectively. The set of Np-Re values fitted the curve provided by the manufacturer.

$$Re = \frac{N \cdot d_{imp}{}^{2} \cdot \rho}{\mu} \quad \text{(eq. 32)}$$

$$N_p = \frac{\dot{Q}_{imp}}{N^3 \cdot d_{imp}{}^{5} \cdot \rho} \quad \text{(eq. 33)}$$

The heat dissipated by the impeller in the most unfavourable case represents 1% against the heat transferred by the coil exchanger. Therefore, it has been neglected for the calculations of the energy stored by the water.

Having neglected the heat loss and the heat dissipated by the impeller, figure 7 shows the energy stored by the TES system with water based on the stirring rate. It can be observed that the energy stored is higher when the stirrer is running, as depicted in figure 3, as the dead volume corresponding to the region 7 has been avoided by the motion caused by the stirrer. In this manner, the thermal energy storage efficiency, defined by equation 34, increased from 85% to 100%. There are no differences in the thermal response depending on the stirring rate, since the overall heat transfer coefficient is almost the same for both rates.

$$\varepsilon_{TES}(t) = \frac{E_{tank\,stored}(t)}{E_{max\,stored}} = \frac{E_{tank\,stored}(t)}{m_{total} \cdot c \cdot \left(\bar{T}_{TES}(t) - T_{TES,0}\right)} \quad \text{(eq. 34)}$$

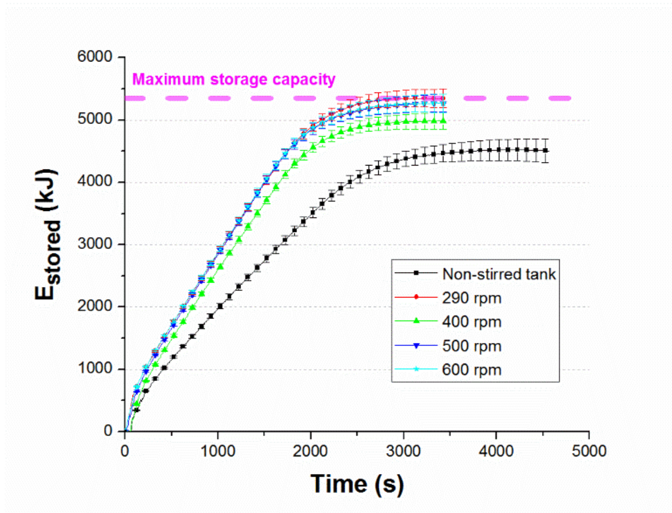

Figure 7. Energy stored by the TES system with water at different stirring rates.

3.3 Tests using a PCM emulsion as thermal storage material

Firstly, the repeatability of the tests using the PCM emulsion was analyzed. Once the repeatability was verified, the test series was started. As an example, figure 8 shows the temperature evolution of the paraffinic emulsion at different heights of the tank, as well as the HTF temperature at the inlet and outlet of the coil, for a test without stirring. In this case, in comparison to the water (figure 2), a larger temperature gradient along the central axis of the tank is observed. As occurred with the water, the temperature recorded by the sensor in position 7 is lower than for the other positions, and even decreases throughout the course of the test due to the ambient losses. It is also observed that from around 4000 seconds, the coil hardly transfers heat, but the temperature of the PCM emulsion in the central axis continues increasing. This behaviour was also observed in some previous works [3, 7]. In order to explain this phenomenon, it would be necessary to use a distributed temperature sensing system to monitor a wider temperature field of the PCM emulsion. During the duration of the test, the PCM emulsions did not reach the inlet temperature of the HTF. When the same test is repeated, but on this occasion activating the stirring, the temperatures of the PCM emulsion along the central axis become uniform, and the PCM emulsion reaches the inlet temperature of the HTF, 60ºC, at around 4000 seconds (see figure 9).

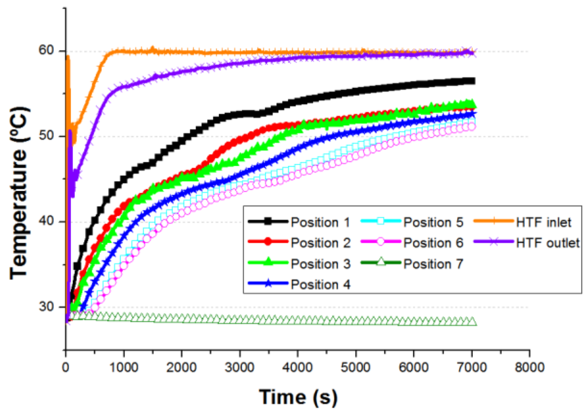

Figure 8. Temperature evolution of the HTF at the inlet and outlet of the coil and temperature evolution of the PCM emulsion inside the tank along the central axis. Flow temperature=60ºC; Mass flow=400 kg/h. No stirring.

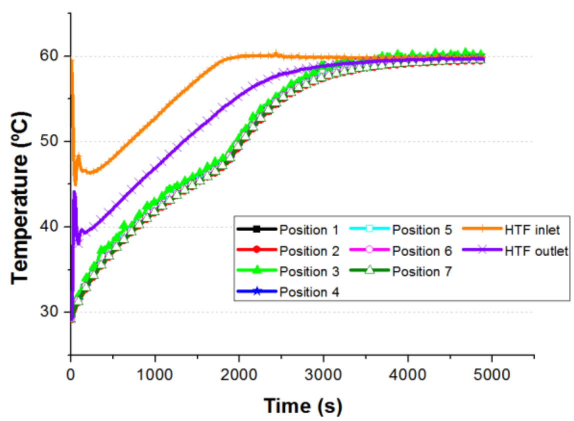

Figure 9. Temperature evolution of the HTF at the inlet and outlet of the coil and temperature evolution of the PCM emulsion inside the tank along the central axis. Flow temperature=60ºC; Mass flow=400 kg/h. Stirring rate=290 rpm.

3.3.1 Obtaining the overall heat transfer coefficient. Comparison to the results with water

Figure 10 shows the results obtained for the PCM emulsion in comparison to water. They have been calculated using the data processing method detailed in section 3.2.1. It can be seen that for the PCM emulsion the overall heat transfer coefficient improved from about 100-150 W/(m^2·K) to 470-680 W/(m^2·K) when stirred with a rotation velocity range from 290 to 600 rpm. It can be said that the stirring enables U values even higher than those for a non-stirred conventional tank with water (U~440 W/(m^2·K)) to be reached even though, as expected, the U values are not as high as when water is stirred (U~1000 W/(m^2·K)). For the PCM emulsion, a higher stirring rate means a higher overall heat transfer coefficient, since under the test conditions the dominant thermal resistance is on the part of the PCM emulsion, unlike the case with water for which no significant improvement is observed when the stirring rate increases. Although not so pronounced, it is also observed that from a PCM emulsion temperature of 45ºC, the overall heat transfer coefficient decreases as result of the viscosity increase from this temperature observed in the previous work [7]. The sharp peak of U in the phase change temperature range reported by Zhang and Niu [8] has not been observed in the present case. Zhang and Niu [8] also reported that with stirring at 380 rpm, the U value was significantly higher for the PCM slurry than for the water even out of the phase change region, a phenomenon not observed in the current work.

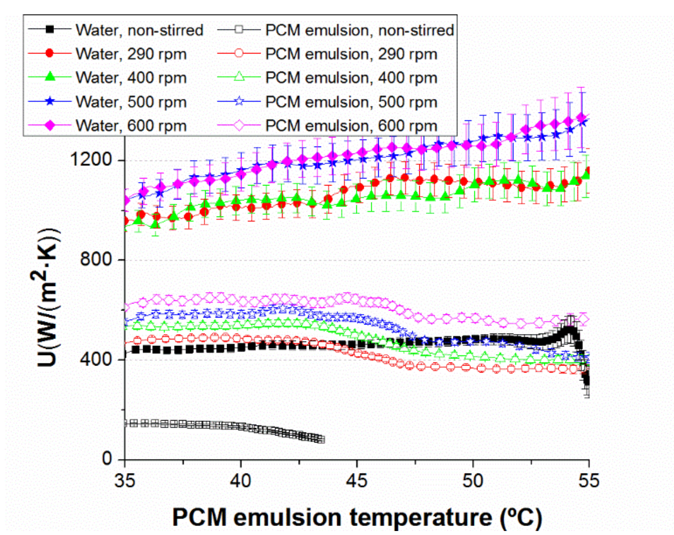

Figure 10. Overall heat transfer coefficient for the PCM emulsion in comparison to water.

As in other experimental works [23-26], the TES system presented here can be modelled and analysed as a heat exchanger between the HTF and the PCM emulsion. Therefore, the effectiveness of the heat exchange process associated to the TES system is described as the ratio of the heat discharged over the theoretical maximum heat that could be discharged. This effectiveness in time can be calculated as defined in equation 35. The effectiveness values presented in table 1 correspond with an average value over the phase change region.

$$\varepsilon_{t_i} = \frac{T_{in,t_i-t_d} - T_{out,t_i}}{T_{in,t_i-t_d} - \lim_{NTU\to\infty} T(L,t_i)} = \frac{T_{in,t_i-t_d} - T_{out,t_i}}{T_{in,t_i-t_d} - T_{TES,x=L_c,t_i}} \quad \text{(eq. 35)}$$

Average effectiveness, $\bar{\mathcal{E}}$ (%)	**Non-stirred**	**290 rpm**	**400 rpm**	**500 rpm**	**600 rpm**
TES with water	46 %	82%	82%	86%	85%
TES with PCM emulsion	17%	53%	58%	61%	64%

Table 1. Effectiveness of the heat exchange process of the TES system with water and with the PCM emulsion at different stirring rates.

Both for the TES system with water and for the TES system with the PCM emulsion, the effectiveness increases when the liquid is agitated. However, it seems that the effectiveness for water remains almost constant with the rotation velocity while an evident increase in its value with the rotation velocity is detected for the PCM emulsion. This is due to the relation between the internal convective heat transfer coefficient (on the part of the HTF) and the external heat transfer coefficient (on the part of the TES fluid). The internal forced convective coefficient is within the range of 2065-2147 W/(m^2·K)). When energy is stored in water, the external convective heat transfer coefficient changes from 2568 to 3671 W/(m^2·K)), depending on the stirring rate. Both thermal resistances are similar and thus a significant improvement is not achieved in spite of increasing the agitation level. In contrast, when the PCM emulsion is used as TES fluid, the external convective heat transfer coefficient changes from 590 to 974 W/(m^2·K)), the external convection being the dominant thermal resistance. For this reason, the effectiveness can still improve with stirring.

3.3.2 Energy stored by the stirred TES system with the PCM emulsion. Comparison with the water tank.

The same procedure as described in Section 3.2.3 was followed for the TES system with the PCM emulsion. Table 2 compiles the results obtained for the different tests, considering the energy stored by the TES system (calculated from the energy balance on the TES system) and the thermal energy storage efficiency calculated according to equation 35. It was observed that both for the water and for the PCM emulsion, when stirring is activated the thermal energy storage efficiency reaches values of 100%, even at the lowest stirring rate. However, due to the non-ad hoc design of the tank without the stirrer running, the TES system with water and with the PCM emulsion reaches a thermal energy storage efficiency of around 85-86% and 76-77%, respectively, within a practical response time for applications. Therefore, with the proposed TES system of a PCM emulsion contained in a conventional tank with a stirrer, even at the lowest stirring rate the energy stored is on average 80% higher than for a conventional tank with water for an operating temperature range from 30-50ºC, and 40% higher for an operating temperature range from 30-60ºC.

	Non-stirred		**290 rpm**		**400 rpm**		**500 rpm**		**600 rpm**	
	ε_{TES} (%)	E_{stored} (kJ)	ε_{TES} (%)	E_{stored} (kJ)	ε_{TES} (%)	E_{stored} (kJ)	ε_{TES} (%)	E_{stored} (kJ)	ε_{TES} (%)	E_{stored} (kJ)
Water 30-60ºC	85%	4510* (55.8ºC)	100%	5320	100%	5090	100%	5280	100%	5350
PCM emulsion 30-60ºC	77%	4910* (49.0ºC)	100%	6290	100%	6470	100%	5890	100%	6050
Water 30-50ºC	86%	2710* (47.1ºC)	100%	3370	100%	3390	100%	3380	100%	3340
PCM emulsion 30-50ºC	76%	3910* (46.3ºC)	100%	4880	100%	5260	100%	5290	100%	5160

Table 2. Storage efficiency and energy stored by the TES system with water and with the PCM emulsion at different stirring rates. *Average fluid temperature between brackets. **The total energy stored differs in spite of reaching a thermal energy storage efficiency of 100% because the initial temperature conditions may have changed slightly.

3.3.3 Heat dissipated by the impeller

Adopting the same procedure as for the water, the heat dissipated by the impeller to the PCM emulsion has been calculated, obtaining results of 4.5, 9.5, 16.5 and 25.0 W for stirring rates of 290, 400, 500 and 600 rpm, respectively. These values have also been checked with the Power number-Reynolds number curve provided by the manufacturer for this type of impeller. In this case, as the PCM emulsion is a pseudoplastic fluid, first an estimation of the average shear rate had to be calculated to obtain a viscosity value, in order to calculate the Reynolds number. Meztner and Otto [27] were the first to establish that for pseudoplastic fluids there appears to be a characteristic average shear rate for a mixer (impeller-tank assembly) which characterizes power consumption, and which is directly proportional to the rotational speed of the impeller (equation 36):

$$\dot{\gamma}_m = k_s \cdot N \quad \text{(eq. 36)}$$

where k_s is a function of the type of impeller and the vessel configuration. If the apparent viscosity corresponding to the average shear rate defined above is used in the equation for a Newtonian liquid, the power consumption is satisfactorily predicted for most non-Newtonian liquids. Skelland [28] compiled experimental values of k_s for a variety of impellers (turbines, propellers, paddles, anchors and so on), and he suggested that for pseudoplastic fluids, k_s lies approximately in the range of 10-13 for most configurations of interest, while slightly larger values of 25-30 have been reported for anchors and helical ribbons [29]. It must be borne in mind that this procedure reduces the complex three-dimensional flow field in a mixing tank to a single constant, k_s.

From the average shear rate, having adopted a k_s value of 11.5, the viscosity of the PCM emulsion was obtained from the flow curve. It was then possible to calculate the Reynolds number according to equation 32. Likewise, the Power number was calculated by means of equation 33. The set of N_p-Re values also fitted the curve provided by the manufacturer. The differences when water was stirred are not very significant, since the PCM emulsion was under conditions of transition from laminar to turbulent flow (Reynolds number from 1000 to 4000 approximately), where the power number starts to become constant.

It must also be pointed out that the motor used in this case is oversized. When the stirred TES tank is to be integrated in a specific application, the application itself will determine the stirring rate so that the system will be capable of supplying the thermal power that the application requires. This will allow for a correct sizing of the motor and will avoid having to purchase a frequency drive, saving both volume and cost for the proposed system.

4. Comparison with other TES systems

As in the previous study [7], the proposed TES system was compared to traditional TES systems using water, and with systems where the PCM is macroencapsulated or in bulk form, confined in the tank, using water as the HTF in the heat exchange. The TES systems were selected from the literature mainly according to their data availability and to their ease of treatment. Furthermore, several encapsulated geometries have been considered with paraffin as the TES material, since the emulsion is of a paraffinic nature. Other TES systems with PCM slurries have also been taken into account. Ice systems, which provide the highest energy density values, have also been included in the comparison. The main characteristics of these TES systems are compiled in table 3.

Ref	Type of encapsulation	Heat storage material	E [kWh/m^3]	U [W/(m^2·K)]	A/V [m^{-1}]	Comments
[31]	a) Double pipe heat exchanger in the annular space	RT35	25.67	30*	11.83	*Approximate U values taken from graphs (melting case)
	b) Same as 1, but with external fins on the copper tube		23.44	60*	69.89	
	c) Compact heat exchanger, with PCM between coil and fins		10.89	50*	193.18	
	d) Plate and frame heat exchanger, with PCM in half of the passages		3.39	15*	875.00	
[32]	Bulk PCM inside Calmac Icebank 1098C	RT8	34.00	35	30.00	
[26]	Bulk PCM inside a tank (prototype)	RT8	35.00	64	22.00	
[33]	Cylindrical capsules (diameter: 7.3 cm; length: 24 cm)	Ice	40.00	65	24.00	
[34]	Spherical capsules (diameter: 7.7 cm)	Ice	46.00	35	47,00	
[1, 30]	Tank with a helical coil inside	a) 20% PCM slurry	20.90*	400**	7.85	*Energy density taken from h-T curves. Temperature range 30-65ºC. Energy density having considered only the heat stored by the material and its volume. **Natural convection coefficient instead of the overall heat transfer coefficient. This should be slightly smaller.
		b) 30% PCM slurry	22.99*	310**	7.85	
		c) 40% PCM slurry	24.73*	230**	7.85	
		d) 50% PCM slurry	26.47*	140**	7.85	
		e) Water (sensible)	17.42*	700**	7.85	
[2]	Tank with a helical coil inside	a) 45% PCM slurry	16.37*	1086**	7.47	*Energy density taken from h-T curves obtained from DSC. Temperature range 2-7ºC. Energy density having considered only the heat stored by the material and its volume. **Natural convection coefficient instead of the overall heat transfer coefficient. This should be slightly smaller.
		b) Water (sensible)	5.81*	717**	7.47	

561 **Table 3.** Characteristics of the different TES systems with which the tank containing the PCM emulsion and water has been compared

To try to establish as rigorous a comparison as possible, three parameters have been compared: the volumetric energy density, the overall heat transfer coefficient (U) and the relation between the heat transfer area and the tank volume (A/V). Figure 11 shows a graphic representation of the results of this comparison, where the new stirred system has been included.

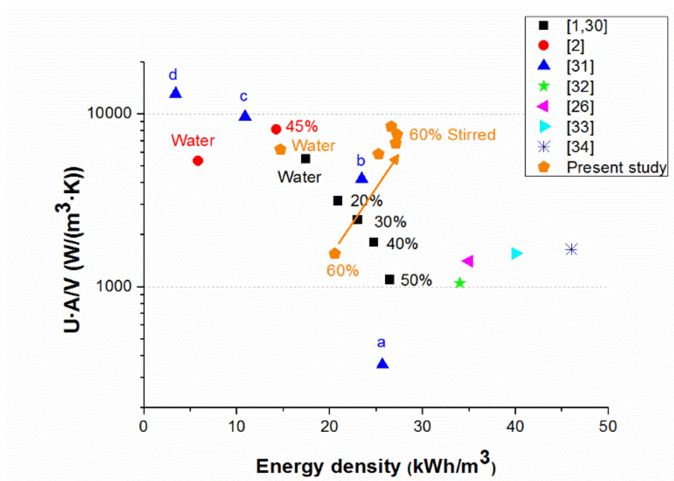

Figure 11. TES systems comparison in terms of volumetric energy density and heat transfer rate

From this comparison, it can be observed that the volumetric energy density of the proposed TES system has improved thanks to the agitation phenomenon, bringing it closer to those values reached in bulk PCM confined in tanks [26, 32]. The thermal power can increase up to five times, as in the TES systems proposed by Medrano et al. [31]. In contrast, they showed a low energy density. Therefore, it can be said that the stirred tank with the PCM emulsion could represent a promising and cost-effective solution.

5. Conclusions

An experimental characterization in terms of the volumetric energy density and heat transfer coefficient of a coiled stirred tank containing a low cost PCM emulsion has been performed. First, the performance was compared depending on whether it was agitated or not, or if it included a sensible TEs material (water) or the PCM emulsion. Secondly, the proposed stirred TES system with the low cost PCM emulsion was compared to traditional and latent TES systems. The main conclusions can be summarized as follows:

1) Dead volumes in the tank are avoided due to the motion caused by the stirrer, improving the thermal energy storage efficiency from 85% to 100% for the water, and from 77% to 100% for the PCM emulsion, even for the lowest rotation velocity.

2) The overall heat transfer coefficient increased from 100-150 W/(m^2·K) to 470-680 W/(m^2·K) with stirring for a rotation velocity range from 290 to 600 rpm for the PCM emulsion. The improvement was not so marked for the water. Nevertheless, it reached a higher value, from 440 to 1000 W/(m^2·K), when the stirrer was running.

3) The effectiveness of the heat exchange shows that for the PCM emulsion, the overall heat transfer coefficient could still be enhanced if the stirring rate is increased.

4) The power consumption of the stirrer is low in comparison to the thermal power exchanged (25 W for the highest stirring rate).

In light of the results of the present investigation, it can be said that the proposed TES system is a promising solution in terms of volumetric energy density and heat transfer against other TES systems analysed in the literature.

Acknowledgements

The authors would like to thank the Spanish Government for funding this work within the framework of the research project (MICINN-FEDER): ENE2014-57262-R. The authors would like to acknowledge the companies Lapesa S.A., RLESA-Repsol and Talleres Garvi for their collaboration in this research. The authors would also like to acknowledge the use of the Servicio General de Apoyo a la Investigación-SAI, Universidad de Zaragoza.

References

[1] Heinz A, Streicher W. Application of phase change materials and PCM-slurries for thermal energy storage, Ecostock Conference, New Jersey (USA) 2006.

[2] Diaconu BM, Varga S, Oliveira AC. Experimental study of natural convection heat transfer in a microencapsulated phase change material slurry. Energy 2010;35(6):2688-93.

[3] Huang MJ, Eames PC, McCormack S, Griffiths P, Hewitt NJ. Microencapsulated phase change slurries for thermal energy storage in a residential solar energy system. Renew Energy 2011;26(11):2932-39.

[4] Vorbeck L, Gschwander S, Thiel P, Lüdemann B, Schossig P. Pilot application of phase change slurry in a 5 m^3 storage. Appl Energy 2013;109:538-43.

[5] Kappels T, Kohnen T, Hanu LG, Pollerberg C. Design and retroffiting of a cold storage replacing water with phase change slurries. Eurotherm Seminar #99. Advances in Thermal Energy Storage.Lérida (Spain), 28-30 May 2014.

[6] Allouche Y, Varga S, Bouden C, Oliveira AC. Experimental determination of the heat transfer and cold storage characteristics of a microencapsulated phase change material in a horizontal tank. Energy Convers Manage 2015;94:275-85.

[7] Delgado M, Lázaro A, Mazo J, Peñalosa C, Dolado P, Zalba B. Experimental analysis of a low cost phase change material emulsion for its use as thermal storage system. Energy Convers Manage 2015;106:201-12.

[8] Zhang S, Niu J. Two performance indices of TES apparatus: Comparison of MPCM slurry vs. stratified water storage tank. Energ Buildings 2016;127:512-20.

[9] http://www.vakkimsa.com/es/agitadores/helices (last access January 2017)

[10] Delgado M, Lázaro A, Mazo J, Marín JM, Zalba B. Experimental analysis of a microencapsulated PCM slurry as thermal storage system and as heat transfer fluid in laminar flow, Appl Therm Eng 2012;36:370-7.

[11] John F. Partial differential equations. 4th edition. Springer-Verlag, New York, 1986.

[12] Kays WM, London AL. Compact heat exchangers. 3th edition. MacGraw-Hill, New York, 1984.

[13] Burdem RL, Faires JD. Numerical analysis. 9th edition. Brooks/Cole, Cengage Learning Boston, 2010.

[14] Ito H. Friction factor for turbulent flow in curved tube. J Basic Eng-T ASME 1959;81:123-34.

[15] Naphon P, Wongwises S. A review of flow and heat transfer characteristics in curved tubes. Renew Sust Energy Rev 2006;10(5)463-90.

[16] Xin RC, Ebadian MA. The effects of Prandtl numbers on local and average convective heat transfer characteristics in helical pipes. J Heat Trans-T ASME 1997;119(3):467-73.

[17] Chabbra RP, Richardson JF. Non-newtonian flow and applied rheology. Engineering Applications. Butterworth-Heinemann/IChemE. 2nd Edition.

[18] Major-Godlewska M. An effect of different factors on heat transfer process in an agitated vessel. Czasopismo Techniczne Chemia 2014;111(2):85-94.

[19] Seth KK, Stahel, EP. Heat transfer from helical coils immersed in agitated vessels. Ind Eng Chem 1969;61(6):39-49.

[20] Dostal M, Verisova M, Petera K, Jirout T, Fort I. Analysis of heat transfer in a vessel with helical pipe coil and multistage impeller. Can J Chem Eng 2014;92:2115-2121.

[21] R.H. Perry, D.W. Green. Perry's Chemical Engineers' Handbook. 7th Edition. McGraw-Hill International Editions 1998. Chemical Engineering Series. Section 18: Liquid-Solid Operations and Equipment.

[22] Ascanio G, Castro B, Galindo E. Measurement of power consumption in stirred vessels- A review. Trans IChemE, Part A, Chem Eng Res Des

[23] Castell A, Belusko M, Bruno F, Cabeza LF. Maximisation of heat transfer in a coil in tank PCM cold storage system. Appl Energ 2011:88:4120-27.

[24] Tay NHS, Belusko M, Bruno F. Experimental investigation of tubes in a phase change thermal energy storage system. Appl Energ 2012:90:288-97.

[25] Tay NHS, Bruno F, Belusko M. Experimental investigation of dynamic melting in a tube-in-tank PCM system. Appl Energ 2013:104:137-48.

[26] López-Navarro A, Biosca-Taronger J, Corberán JM, Peñalosa C, Lázaro A, Dolado P, Payá J. Performance characterization of a PCM storage tank. Appl Energ 2014:119:151-62.

[27] Metzner AB, Otto RE. Agitation of non-Newtonian fluids. AIChE J 1957:3(1):3-10.

[28] Skelland AHP. Handbook of Fluids in Motion (edited by NP Cheremisinoff and R Gupta). Ann Harbor Science 1983: Chapter 7.

[29] Bakker A, Gates LE. Viscous Mixing. Chem Eng Prog 1995:91(12):25-34.

[30] Streicher W, Heinz A, Puschnig P, Schranzhofer H, Eisl G, Heimrath R, Wallner G, Schobermayr H. Fortschrittliche Wärmespeicher zur Erhöhung von solarem Deckungsgrad und Kesselnutzungsgrad sowie Emissionsverringerung durch verringertes Takten. Projektzum IEA-SHC Task 32, 2006.

[31] Medrano M, Yilmaz MO, Nogués M, Martorell I, Roca J, Cabeza LF. Experimental evaluation of commercial heat exchangers for use as PCM thermal storage systems. Appl Energ 2009;86(10):2047-55.

[32] Torregrosa-Jaime B, López-Navarro A, Corberán JM, Esteban-Matías JC, Klinkner L, Payá J. Experimental analysis of a paraffin-based cold storage tank. Int J Refrig 2013;36(6):1632-40.

[33] Chen S, Chen C, Tin C, Lee T, Ke M. An experimental investigation of cold storage in an encapsulated thermal storage tank. Exp Therm Fluid Sci 2000;23(3-4):133-44.

[34] Bédécarrats JP, Strub F, Falcon B, Dumas JP. Phase-change thermal energy storage using spherical capsules: performance of a test plant. Int J Refrig 1996;19(3):187-96.

Figure captions

Figure 1. Arrangement of the Pt100 sensors inside the tank

Figure 2. Temperature evolution of the HTF at the inlet and outlet of the coil and temperature evolution of the water inside the tank along the central axis. Flow temperature=60ºC; Mass flow=400 kg/h. No stirring.

Figure 3. Temperature evolution of the HTF at the inlet and outlet of the coil and temperature evolution of the water inside the tank along the central axis. Flow temperature=60ºC; Mass flow=400 kg/h. Stirring at 290 rpm.

Figure 4. Overall heat transfer coefficients for the water without stirring (natural convection) and stirring at 290, 400, 500 and 600 rpm.

Figure 5. Dimensionless experimental results vs.fitting correlation.

Figure 6. Comparison of the fitting correlation with other correlations taken from the literature.

*The correlation for the paddle impeller is not visible, because it is overlapped by the correlation for the anchor impeller.

Figure 7. Energy stored by the TES system with water at different stirring rates.

Figure 8. Temperature evolution of the HTF at the inlet and outlet of the coil and temperature evolution of the PCM emulsion inside the tank along the central axis. Flow temperature=60ºC; Mass flow=400 kg/h. No stirring.

Figure 9. Temperature evolution of the HTF at the inlet and outlet of the coil and temperature evolution of the PCM emulsion inside the tank along the central axis. Flow temperature=60ºC; Mass flow=400 kg/h. Stirring rate=290 rpm.

Figure 10. Overall heat transfer coefficient for the PCM emulsion in comparison to water.

Figure 11. TES systems comparison in terms of volumetric energy density and heat transfer rate

Table captions

Table 1. Effectiveness of the heat exchange process of the TES system with water and with the PCM emulsion at different stirring rates.

Table 2. Storage efficiency and energy stored by the TES system with water and with the PCM emulsion at different stirring rates. *Average fluid temperature between brackets. **The total energy stored differs in spite of reaching a storage efficiency of 100% because the initial temperature conditions may have changed slightly.

Table 3. Characteristics of the different TES systems with which the tank containing the PCM emulsion and water has been compared.